Ultra-Broadband Spectrally Selective Absorber for Solar Thermal Absorption Based on TiN Square-Ring Meta-Structure

Ziang Gao, Shilin Yu, Zihao Li, Dafa Pan, Zhengshan Xu, and Tonggang Zhao

***Abstract*—Based on the TiN square-ring structure, a spectrally selective absorber for solar thermal absorption is proposed announcing an average absorption of 95.69% in the major solar spectral region (280 nm∼2500 nm). When the wavelength exceeds 2500 nm, the absorption declines rapidly and decreases to 40.4% at the wavelength of 4000 nm, showing excellent spectral selectivity. As the incident angle of TE or TM polarized wave varies in a range of 0∼60 degrees, the proposed absorber maintains more than 90% solar absorption efficiency, which proves the insensitivity of incident angle and polarization angle. With operating temperature T = 300 K and solar concentrating coefficient C = 1, the solar-thermal conversion efficiency of the proposed absorber is 93.92%. At a high temperature of 700 °C, the solar-thermal conversion efficiency can maintain more than 80% at the condition of C = 200, demonstrating good thermal tolerance. It is believed that the proposed absorber has great potential to be applied in solar thermal absorption systems.**

***Index Terms*—Solar thermal absorption, ultra-broadband absorber.**

I. Introduction

IN MODERN society, excessive use of traditional energy which is a non-renewable resource has led to lots of environmental problems [1], [2]. With the continuous development of society, its reserves will continue to decrease, so how to reduce dependence on traditional energy has become a hot social concern. Solar energy is a kind of abundant and renewable clean energy. The efficient use of solar energy can effectively solve various problems in modern society. Compared with the traditional solar photovoltaic system, the solar thermal system has been widely concerned by society because of its higher energy conversion efficiency and better utilization of solar energy.

Manuscript received 11 October 2022; revised 24 November 2022; accepted 7 December 2022. Date of publication 12 December 2022; date of current version 30 December 2022. This work was supported in part by the National Natural Science Foundation of China under Grant 61835002 and in part by BUPT Innovation and Entrepreneurship Support Program under Grant 2022-YC-A060. *(Corresponding author: Tonggang Zhao.)*

Ziang Gao and Shilin Yu are with the School of Electronic Engineering, Beijing University of Posts and Telecommunications, Beijing 100876, China, and also with the Beijing Key Laboratory of Space-Ground Interconnection and Convergence, Beijing University of Posts and Telecommunications, Beijing 100876, China (e-mail: zagao@bupt.edu.cn; yushilin@bupt.edu.cn).

Zihao Li, Dafa Pan, Zhengshan Xu, and Tonggang Zhao are with the School of Electronic Engineering, Beijing University of Posts and Telecommunications, Beijing 100876, China (e-mail: zihaoli@bupt.edu.cn; pandafa@bupt.edu.cn; hyxzs@bupt.edu.cn; zhaotg@bupt.edu.cn).

Digital Object Identifier 10.1109/JPHOT.2022.3228580

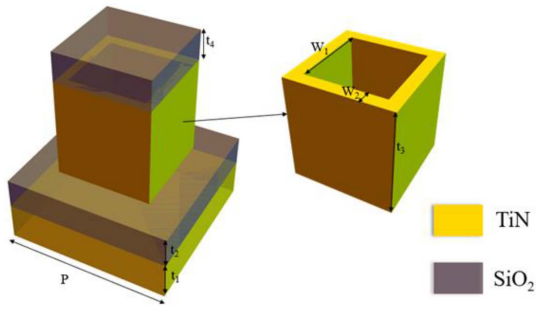

Fig. 1. Schematic diagram of the unit structure of the designed absorber.

A solar spectrally selective absorber is the core component of the solar thermal system which directly affects the energy conversion efficiency of the system. In addition to the basic performance of the traditional broadband absorber, solar absorber, as a kind of broadband absorber, is also required to have excellent spectral selectivity which is important to high absorption in solar spectra and low loss of thermal radiation emissivity in the mid-infrared band. With the deep research on metamaterial and surface plasmon, wideband absorbers with excellent spectral selectivity and insensitivity to polarization and incidence angle have been proposed one by one [3], [4], [5], [6], [7], which is expected to be applied in the design of solar absorbers. Further, kinds of solar spectrally selective absorber structures such as multilayer metal/insulator/metal structure [8], [9], [10], [11], [12], fishnet gratings [13], [14], [15], [16], moth eye [17], [18], [19], and ring structure [20], [21], [22], [23] have been studied for solar thermal absorption.

In this paper, we proposed a solar spectrally selective absorber for solar thermal absorption which is composed of periodic TiN nano-square rings, and its unit schematic is shown in Fig. 1. The substrate is composed of TiN and SiO_2. The SiO_2 insulator is filled in the middle of the cavity formed by the TiN nano-square ring, which can improve the stability of the structure and make it not susceptible to the influence of the surrounding environment. In addition, from the perspective of optical characteristics, the filling of SiO_2 insulator also improves the absorption performance of the structure.The average absorptivity of the absorber in the wavelength range of 280∼2500 nm is about 95.69%. The mechanism by which the structure achieves broadband high absorption is studied by electromagnetic field distribution. After calculation, the energy conversion efficiency is 94.76%

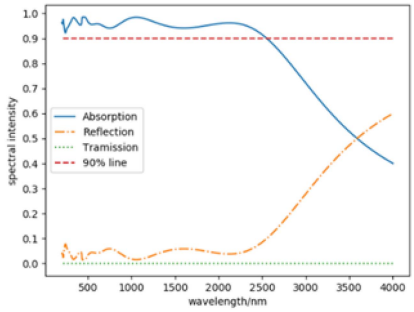

Fig. 2. Absorption spectra of the designed absorber in the band of 200 nm∼4000 nm.

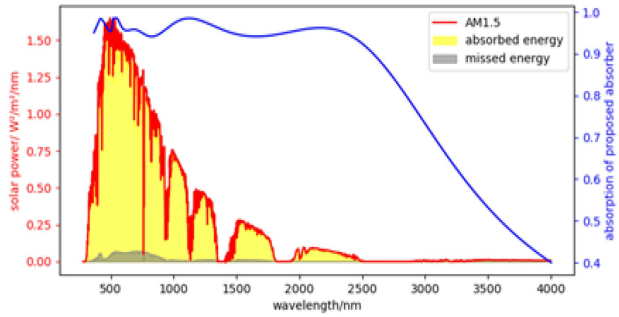

Fig. 3. Solar radiation spectrum and solar absorption of the proposed absorber in the band range of 200 nm∼4000 nm.

when the solar concentration coefficient C = 1 and the working temperature is 300 K. In addition, we also calculated the effect of structural parameters on the absorption performance. In addition, we also investigated the effect of different polarizations and incident angles on the absorption performance. The results show that the absorber has the advantages of polarization independence and angle insensitivity to incidence.

II. Analysis of Absorption Performance

During numerical calculation, the thickness of TiN substrate is $t_1 = 100$ nm, the thickness of the lower SiO_2 insulator is $t_2 = 80$ nm, the height of the nano-square ring is $t_3 = 260$ nm, the inner side length is $W_1 = 190$ nm, the thickness $W_2 = 25$ nm, the thickness of the top anti-reflection layer is $t_4 = 70$ nm, and the unit structure period is P = 410 nm. In the experimental preparation, the proposed structure can be prepared by deposition and photolithography, reactive magnetron sputtering, chemical vapor deposition, and atomic layer deposition.

In this paper, the numerical calculation method of the optical characteristics is the finite-difference time-domain (FDTD) method. The boundary condition of the structure in the z direction is set as the perfect matching layer (PML), and the boundary condition in the x and y directions are set as periodic boundary conditions, respectively. In addition, the mesh step is set as 5 nm. The incident light source is a plane electromagnetic wave that incident vertically on the surface of the structure. The dielectric constants of TiN and SiO_2 are obtained from [24].

The spectral absorption of metamaterial structures is defined as follows [25]:

$$A\ (\lambda) = 1 - R\,(\lambda) - T\,(\lambda) \tag{1}$$

where $R(\lambda)$ and $T(\lambda)$ is the reflection and transmission spectra of the absorber under the incidence of an external electromagnetic wave, and λ represents the incident wavelength. In order to achieve maximum absorption, the electromagnetic wave reflection and transmission should be minimized. Since the thickness of TiN substrate is 100 nm, which is far beyond the skin depth [26], [27], the transmission spectrum of the structure is almost 0, and (1) can be simplified as:

$$A(\lambda) = 1 - R(\lambda) \tag{2}$$

Fig. 2. shows the absorption spectrum of the designed absorber under the vertical incident TM polarized wave. It can be seen that the absorption is above 90% in the band of 280 nm∼2500 nm, in which the solar radiation energy is the most concentrated. The average absorption in this band is 95.69%, so the designed absorber can absorb solar radiation energy well. When the wavelength is 495 nm, the absorption peak reaches 98.55%, and the absorption begins to decline after the wavelength of 2500 nm. When the wavelength is 4000 nm, the absorption decreases to 40.4%, showing good spectral selectivity.

In terms of absorption performance, a solar thermal absorber should not only efficiently absorb sunlight in the ultraviolet to the near-infrared band to achieve high solar absorption efficiency α, but also have a low emissivity ε in the mid-infrared band to prevent thermal energy loss. The calculation equation of α and ε is as follows [28]:

$$\alpha = \frac{\int_{0.28\mu m}^{2.5\mu m} I_{AM1.5}(\lambda)A(\lambda)d\lambda}{\int_{0.28\mu m}^{2.5\mu m} I_{AM1.5}(\lambda)d\lambda} \tag{3}$$

$$\varepsilon = \frac{\int_{2.5\mu m}^{20\mu m} I_B(\lambda,T)A(\lambda)d\lambda}{\int_{2.5\mu m}^{20\mu m} I_B(\lambda,T)d\lambda} \tag{4}$$

where $I_{AM1.5}(\lambda)$ is the spectral intensity of solar radiation in air mass of 1.5, and its spectral figure is shown in Fig. 3(red line). Since solar energy is mainly concentrated in the ultraviolet to the near-infrared band, the range of integration in (3) is 280 nm to 2500 nm to calculate solar absorption efficiency. $I_B(\lambda, T)$ represents the spectral intensity of blackbody radiation at temperature T, which can be calculated by the following equation [29]:

$$I_B\,(\lambda, T)\ = \frac{2\pi hc^2}{\lambda^5}\ \cdot \frac{1}{e^{hc/\lambda kT} - 1} \tag{5}$$

where h is Planck's constant and $h = 6.6260693 \times 10^{-34} J \cdot s$, c is the speed of light, k is Boltzmann's constant and $k = 1.380649 \times 10^{-23} J/K$, and T is blackbody temperature.

Through (3)–(5), the solar absorption efficiency and the emissivity in the mid-infrared band of the proposed absorber are calculated, as shown in Figs. 3. and 4. In the ultraviolet to the near-infrared band, the solar absorption efficiency α of the proposed absorber is 95.75%, while in the near-infrared to mid-infrared band, the energy emissivity ε is 12.67%.

The solar-thermal conversion efficiency is an important index to measure a spectrally selective solar absorber which can be

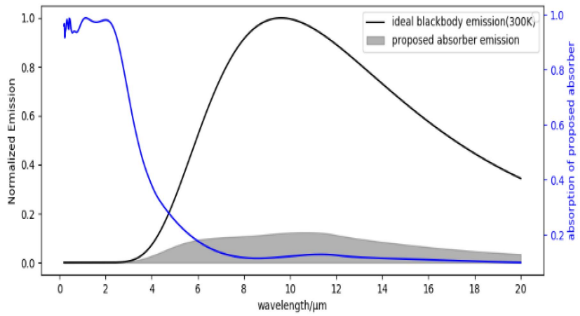

Fig. 4. Ideal blackbody radiation spectrum and energy emissivity of the proposed absorber at 300 K.

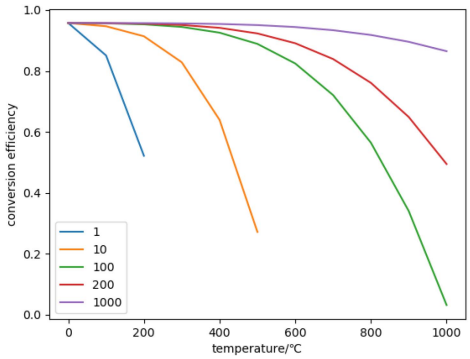

Fig. 5. Curves of solar-thermal conversion efficiency versus temperature of the proposed absorber under different solar concentrating coefficients.

calculated by the following equation [30]:

$$\eta = \frac{\alpha G - \varepsilon\left(\sigma T^4 - \sigma T_0^4\right)}{G} \tag{6}$$

where G is the total incident radiation, which can be expressed as $G = C \times 1000 W/m^2$ [31], C is the solar concentrating coefficient, σ is the Stepan-Boltzmann constant and $\sigma = 5.67 \times 10^{-8} W/(m^2 \cdot K^4)$, T is the operating temperature of the absorber, T_0 is the atmospheric temperature which is agreed to be 273 K. When C = 1 and T = 300 K, the solar-thermal conversion efficiency η of the proposed absorber is calculated to be 93.92%.

In addition, the performance of the absorber under different C and different T are calculated, as shown in Fig. 5. When C is 200, η maintains more than 80% in the range of 0∼700 °C and η is 76.09% even at a high operating temperature of 800 °C, which is still nearly close to 80%. When C is 100, the conversion efficiency is obviously lower than that when C is 200. With the increase of T in the range of 0∼1000 °C, η decreases significantly. However, even at 600 °C, η is 82.45%, which still remains above 80%. Based on the above data, the proposed absorber can maintain a high solar-thermal conversion efficiency at different temperatures, so it can adapt to various environments and has the possibility of practical application.

Considering the randomness of incident sunlight, it is necessary to study the sensitivity to polarization and incident angle of the proposed absorber. As shown in Fig. 6, when light incident vertically on the structure surface, due to the periodic symmetry

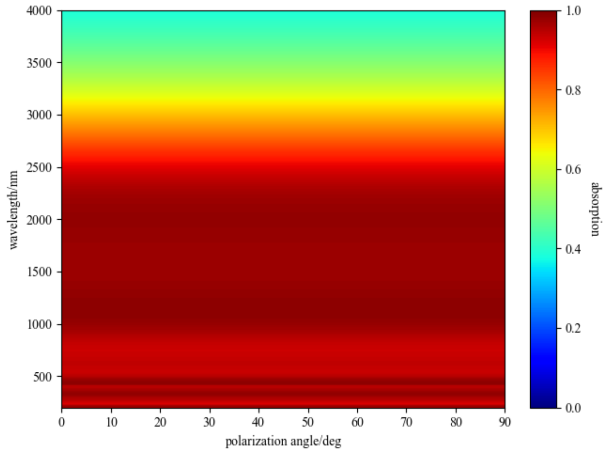

Fig. 6. Absorption spectra of the proposed absorber at different polarization angles under vertical incident wave.

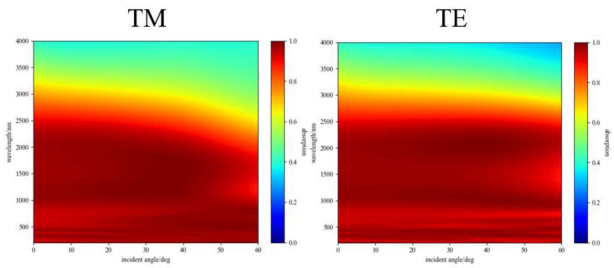

Fig. 7. Absorption spectra when TM and TE polarized wave incident on the proposed absorber at different incident angles.

of the structure, the absorption of incident light at different polarization angles is almost the same, showing excellent polarization insensitivity. When discussing the influence of different incident angles on absorption performance, the absorption of TE and TM polarized waves should be considered respectively. Fig. 7 shows the absorption spectrum of the absorber when the incident angle varies from 0° to 60°. It can be seen from the figure that with the increase of the incident angle, the absorption bandwidth of the structure gradually becomes narrower, and the absorption of the longer band decreases, while that of the shorter band increases slightly. When the incident angle of the TM polarized wave varies from 0° to 20°, the absorption curve of the structure nearly does not change. When the incident angle is 40°, the absorption of the absorber can still maintain more than 90% in 280 nm∼2200 nm. When the incident angle is increased to 60°, the average absorption of the proposed absorber at 280 nm∼2500 nm is 89.04%, and the solar absorption efficiency is 95.46%, which is almost consistent with the solar absorption efficiency at vertical incidence. For TE-polarized waves whose incident angle varies from 0° to 60°, the absorption, and bandwidth of the absorber decrease with the increase of the incident angle. When the incident angle is 50°, the absorption can be maintained above 90% from 280 nm to 2500 nm. When the incident angle is 60°, although the absorption of some bands in the range of 280 nm∼2500 nm is below 90%, the average absorption of the absorber in this band range is 92.77%, and the solar absorption efficiency is 93.79%, which is only 1.96%

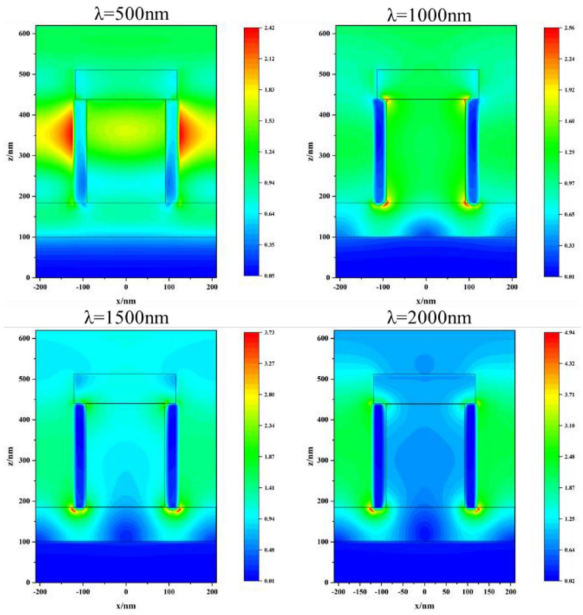

Fig. 8. Electric field distribution in x-z plane when vertical incidence of TM polarized wave under different wavelength. (The boundary of SiO_2 insulator has been marked with a solid line frame.).

different from that of the vertical incident. Based on the above data, it can be shown that the proposed absorber is insensitive to the incident angle and polarization angle.

III. Analysis of Electric Field Distribution

In order to further study the absorption mechanism of the proposed absorber, the distributions of the electric field under different wavelengths of incident wave are analyzed. Judging by the electric field distribution, it can be included that light incidents after SiO_2 anti-reflection then into the TiN-square-ring full of SiO_2. In relatively short wavelengths, cavity structure produces resonance under the excitation of incident light and the resonance also occurs between unit structures. At the longer wavelength, TiN and SiO_2 excite surface plasmon resonance under the action of incident light. The absorption mechanism at each wavelength jointly contributed to the high absorption of the absorber in 280 nm∼2500 nm. In order to study the response characteristics of the absorber more specifically, the electric field distribution of the absorber at the wavelength of 500 nm, 1000 nm, 1500 nm, and 2000 nm are calculated, as shown in Fig. 8. As can be seen, when the wavelength is 500 nm, the incident light passes through the SiO_2 anti-reflection layer and enters into the TiN cavity. After scattering by the SiO_2 insulator filled in the square ring, the cavity resonance is generated and the electric field in the TiN ring forms a standing wave, so the electric field is bound to the center of the square ring, which leads to energy consumption and promotes the high absorption. In addition, at the wavelength of 500 nm, Fabry-Perot resonance is generated between the cell structures [32], which makes the electric field significantly enhanced in the center of the two parallel TiN plates of the unit structure. Surface plasmons resonance can be excited on the TiN surface because of its metallic dielectric

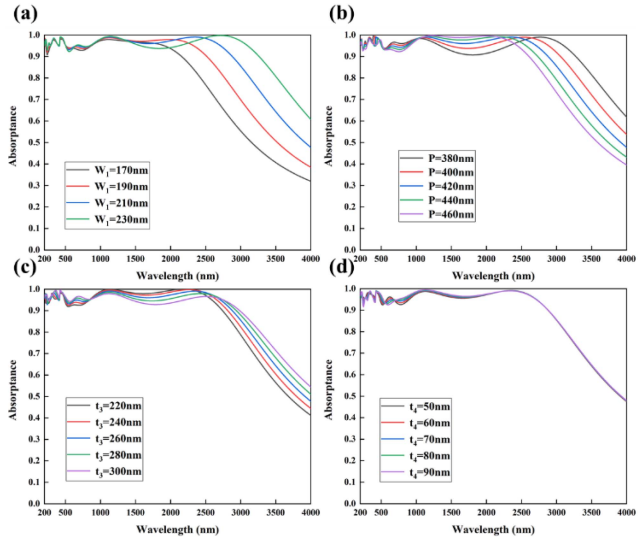

Fig. 9. Absorption spectrum of proposed absorber with different (a) inner side length of square ring W_1 (b)unit period P (c)height of square ring t_3 (d)thickness of anti-reflection layer t_4.

constant in the visible light to the near-infrared band [33]. At the wavelength of 1000 nm, 1500 nm and 2000 nm, incident light excites Localized Surface Plasmon Resonance (LSPR) of the TiN square ring structure. As shown in the Fig. 8, by observing the distribution of the electric field, we can find that these local surface plasmon for the excitement tend to gather to the tips and the edges, forming a strong local area field enhancement. In the nearby area, a large electric field enhancement is formed.

IV. Influence of Different Parameters on Absorption Performance

Fig. 9(a) shows the influence of different inner side lengths of square ring W_1 on absorption characteristics. Change of W_1 might affect the excitation and coupling of surface plasmon polaritons. With the decrease of the W_1, the coupling ability between free electrons on the metal surface and incident electromagnetic wave will be weakened. Therefore, it can be seen from the figure that the high absorption bandwidth gradually gets narrower with the decrease of W_1, and the absorption at the longer band also decreases to some extent. In addition, with the increase of W_1, the absorption of the lower band decreases slightly, because the increase of inner diameter of cavity weakens the resonance of cavity mode. When W_1 gets larger, the absorption of some bands drops below 90%. When W_1 is 190 nm, the absorption bandwidth covers the concentrated band of solar radiation, and the absorption of the lower band is above 90%, so 190 nm is the best size of W_1. Fig. 9(b) shows the influence of different unit period P on absorption characteristics, with the increase of P, the duty ratio between unit structure increases, the coupling of all modes between unit structure decreases and leads to narrower bandwidth and high absorption. In the 500 nm∼800 nm band, with the decrease of P, the interval of the unit structure increases, leading to stronger Fabry-Perot resonance and larger absorption. When P is 420 nm, the proposed absorber has the best absorption performance.

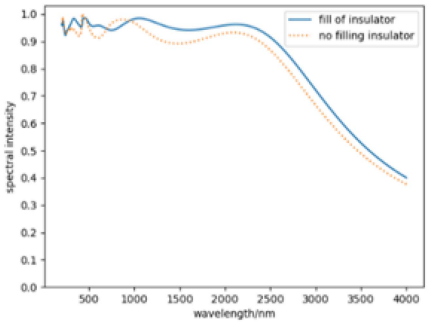

Fig. 10. Absorption spectrum of proposed absorber with/without filling SiO_2 insulator in the square ring.

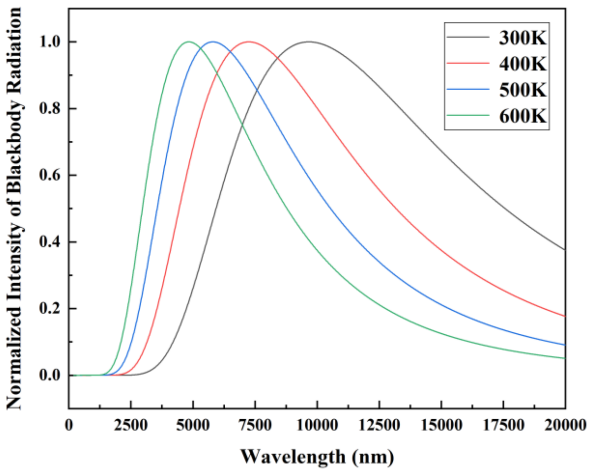

Fig. 11. Black body radiation energy density at different temperatures (from 300 K to 600 K).

Fig. 9(c) shows the influence of different t_3 on absorption characteristics. This parameter might affect the resonance of the cavity mode in the square ring. With the increase of t_3, the absorption in the shorter wave increases, while the absorption in the longer band decreases. The performance of the structure is optimal when t_3 is 260 nm. Fig. 9(d) shows the influence of t_4 on absorption characteristics. This parameter will affect the incident environment when the incident wave enters the square ring and also affect the impedance of the absorber. As can be seen from the figure, with the increase of t_4, the absorption of the structure is improved, but when t_4 increases to a certain extent, the influence on absorption characteristics of the absorber will gradually weaken. Considering the difficulty of manufacturing process, t_4 is finally set as 70 nm. Fig. 10 shows the absorption spectrum of the proposed absorber with or without filling SiO_2 insulator in a square ring. On the whole, the absorption of structure filled with SiO_2 insulator is higher. This is because the presence of the interface between metal and insulator makes the generation of surface plasmon resonance more easily. Therefore, the presence of SiO_2 in the square ring makes the structure has a stronger binding effect on electromagnetic fields, thus improving the absorption.

We analyzed the spectrum of black body radiation energy density at different temperatures. As shown in Fig. 11, it can be seen that as the temperature rises, the energy density curve will produce a blue shift. It will cause energy loss due to heat radiation in the shorter wavelengths.

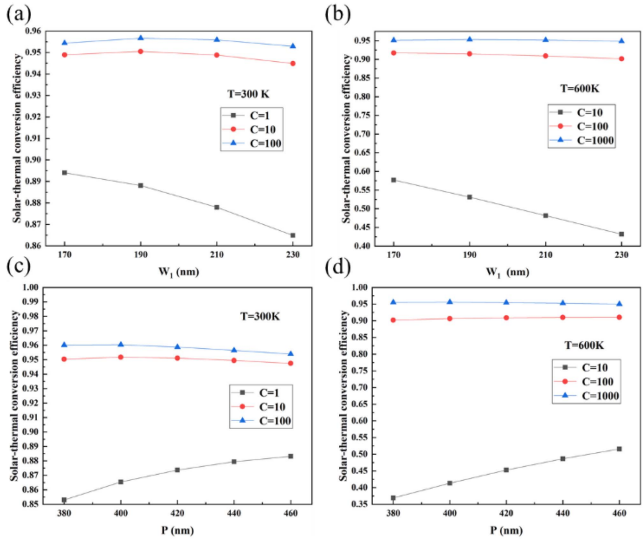

Fig. 12. Solar-thermal conversion efficiency at different temperatures and different light collection intendity for structural parameter W_1 and P.

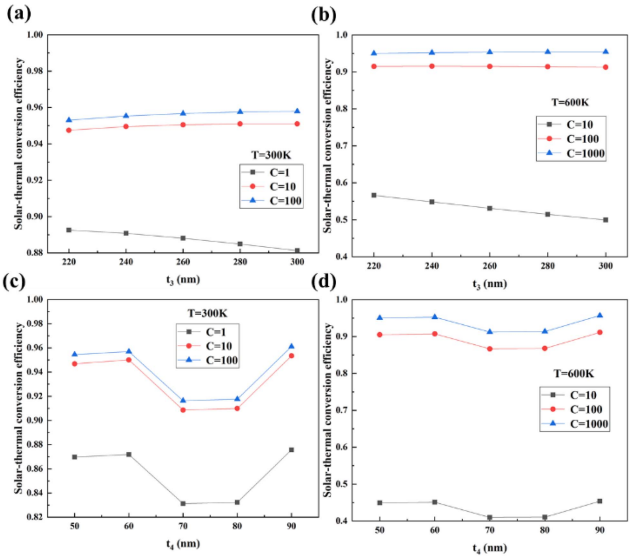

Fig. 13. Solar-thermal conversion efficiency at different temperatures and different light collection intendity for structural parameter t_3 and t_4.

Considering the high temperature in the actual application scene, we considered the wavelength from 200 nm to 20um for the calculation of ε as shown in Fig. 12. After optimization analysis and calculation, when $W_1 = 190$ nm, P = 420 nm, t3 = 260 nm $t_4 = 90$ nm, the maximum average absorption rate is 96.2%. (The equation of ε is used as following:)

$$\varepsilon = \frac{\int_{0.2\mu m}^{20\mu m} I_B(\lambda, T) A(\lambda) \, d\lambda}{\int_{0.2\mu m}^{20\mu m} I_B(\lambda, T) \, d\lambda} \tag{7}$$

By analyzing the above data in Figs. 12 and 13 , we obtained the structural parameters corresponding to the maximum solar thermal energy conversion efficiency (96.11%) at 300 K (C = 100): $W_1 = 190$ nm, P = 420 nm, t3 = 260 nm $t_4 = 90$ nm.

TABLE I
PERFORMANCE COMPARISON TO OTHER ABSORBERS

Reference	Wavelength (nm)	Bandwidth (nm)	Average absorption (%)	Solar-thermal conversion efficiency (%)	Incident angle (°)	Polarization independence
[34]	500-1800	1300	85.4	\	65	No
[35]	280-4000	3720	91	\	\	\
[36]	400-750	350	90	\	60	Yes
[37]	480-1480	1000	90	\	60	Yes
[38]	386-1178 (TE) 300-1140 (TM)	792 (TE) 840 (TM)	97	96 (373-779K)	60 (TE) 50 (TM)	No
[39]	400-2500	2100	97.6	\	60	Yes
[40]	400-2000	1600	91	\	76	No
[41]	300	2210	99	96.45	\	\
Proposed	280-2500	2220	95.69	93.92 (300K)	60	Yes
Improved	280-2500	2220	96.2	96.11 (300K)	60	Yes

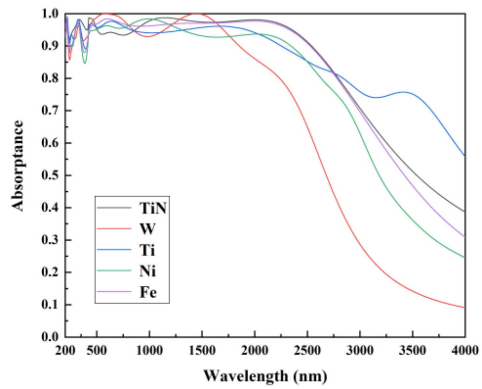

Fig. 14. Absorption spectrum of proposed absorbers with different materials.

Simultaneously, maximum solar thermal energy conversion efficiency (95.69%) at 600 K (C = 1000): W_1 = 190 nm, P = 420 nm, t_3 = 260 nm, t_4 = 90 nm.

As a new type of refractory, TiN has a melting point of 2930 °C and good high-temperature durability. The application of TiN materials can solve the problems of high cost, low melting point and poor stability of absorber materials previously studied, and TiN has the characteristics of compatibility with the CMOS process, adjustable dielectric constant, and strong stability. In the visible and near-infrared bands, the imaginary part of the dielectric constant of TiN is high, which has a large optical loss compared with precious metals, and can show plasma resonance characteristics. As shown in Fig. 14, we compared TiN with other materials.

Finally, the performance of the proposed absorber compared with other recently published absorbers is investigated, as shown in Table I. Compared with other literatures, the working band has been broadened to a large extent, and the application range is wider. The performance of the absorber in the literature has an advantage in a certain index, but in general, the improved absorber achieves high absorption rate, high conversion efficiency and independence of large angle of incident and polarization at the same time.

V. CONCLUSION

We proposed a SiO_2-filled and anti-reflection-coated nano-TiN-square-ring structure that can be applied for solar thermal absorption under high temperatures. Localized surface plasmon resonance (LSPR), magnetic polariton, and cavity mode are excited in the structure, leading to high absorption and ultrawide work band. Because of proved spectral selectivity, the structure has high solar absorption efficiency in the major solar spectral region, low thermal emissivity in the mid-infrared region, and thus high solar-thermal conversion efficiency. The structure is demonstrated as insensitive to incident angle and polarization angle, so it can be applied in different lighting environments. The nano-TiN-square-ring-based structure has a simple geometry so that relatively simple procedure for its production, showing the potential application in the solar thermal field.

REFERENCES

[1] S. Chu, Y. Cui, and N. Liu, "The path towards sustainable energy," *Nature Mater.*, vol. 16, no. 1, pp. 16–22, 2016, doi: 10.1038/nmat4834.
[2] F. Creutzig, P. Agoston, J. C. Goldschmidt, G. Luderer, and R. C. Pietzcker, "The underestimated potential of solar energy to mitigate climate change," *Nature Energy*, vol. 2, no. 9, pp. 1–9, 2017, doi: 10.1038/nenergy.2017.140.
[3] Y. Li, Z. Liu, H. Zhang, P. Tang, B. Wu, and G. Liu, "Ultra-broadband perfect absorber utilizing refractory materials in metal-insulator composite multilayer stacks," *Opt. Exp.*, vol. 27, 2019, Art. no. 11809, doi: 10.1364/OE.27.011809.
[4] D. Sang et al., "Toward high-efficiency ultrahigh numerical aperture freeform metalens: From vector diffraction theory to topology optimization," *Laser Photon. Rev.*, vol. 16, 2022, Art. no. 2200265, doi: 10.1002/lpor.202200265.
[5] Z. Liu, G. Liu, X. Liu, Y. Wang, and G. Fu, "Titanium resonators based ultra-broadband perfect light absorber," *Opt. Mater.*, vol. 83, pp. 118–123, 2018, doi: 10.1016/j.optmat.2018.06.008.

[6] W. Ma, S. Yu, and T. Zhao, "Numerical study of an ultra-broadband perfect absorber from ultraviolet to near-infrared based on metal quadruple staircase structure," *Opt. Commun.*, vol. 493, 2021, Art. no. 127037, doi: 10.1016/j.optcom.2021.127037.

[7] P. Nochian and Z. Atlasbaf, "A novel single layer ultra-wideband metamaterial absorber," *Prog. Electromagn. Res. Lett.*, vol. 93, pp. 107–114, 2020, doi: 10.2528/PIERL20011406.

[8] D. Wu et al., "Numerical study of an ultra-broadband near-perfect solar absorber in the visible and near-infrared region," *Opt. Lett.*, vol. 42, pp. 450–453, 2017, doi: 10.1364/OL.42.000450.

[9] S. Mehrabi, M. H. Rezaei, and A. Zarifkar, "Ultra-broadband solar absorber based on multi-layer TiN/TiO2 structure with near-unity absorption," *J. Opt. Soc. Amer. B Opt. Phys.*, vol. 36, pp. 2602–2609, 2019, doi: 10.1364/JOSAB.36.002602.

[10] W.-X. Zhou et al., "Nano-Cr-film-based solar selective absorber with high photo-thermal conversion efficiency and good thermal stability," *Opt. Exp.*, vol. 20, pp. 28953–28962, 2012, doi: 10.1364/OE.20.028953.

[11] X. Jiang, L. Zhou, J. Hu, and T. Wang, "Nanostructured multilayer hyperbolic metamaterials for high efficiency and selective solar absorption," *Opt. Expres*, vol. 30, pp. 11504–11513, 2022, doi: 10.1364/OE.451849.

[12] J. Liu, Z.-Q. Sun, and H. Wang, "Design and characterization of solar absorbing multilayer stack based on Al/Cr-N-O/SiO_2 layers," *Sol. Energy Mater. Sol. Cells*, vol. 188, pp. 18–26, 2018, doi: 10.1016/j.solmat.2018.06.013.

[13] Q. Liang, H. Duan, X. Zhu, X. Chen, and X. P. Xia, "Solar thermal absorber based on dielectric filled two-dimensional nickel grating," *Opt. Mater. Exp.*, vol. 9, pp. 3193–3203, 2019, doi: 10.1364/OME.9.003193.

[14] H. Li et al., "Broadband selective solar absorber based on dielectric-filled anti-reflection coated film-coupled two-dimensional metallic photonic crystals," *Japanese J. Appl. Phys.*, vol. 57, 2018, Art. no. 110303, doi: 10.7567/jjap.57.110303.

[15] Q. Liang, Q. Yin, L. Chen, Z. Wang, and X. Chen, "Perfect spectrally selective solar absorber with dielectric filled fishnet tungsten grating for solar energy harvesting," *Sol. Energy Mater. Sol. Cells*, vol. 215, 2020, Art. no. 110664, doi: 10.1016/j.solmat.2020.110664.

[16] J. B. Chou et al., "Design of wide-angle selective absorbers/emitters with dielectric filled metallic photonic crystals for energy applications," *Opt. Exp.*, vol. 22, pp. A144–A154, 2014, doi: 10.1364/OE.22.00A144.

[17] H. Wang and L. Wang, "Perfect selective metamaterial solar absorbers," *Opt. Exp.*, vol. 21, pp. A1078–A1093, 2013, doi: 10.1364/OE.21.0A1078.

[18] H. Liu, M. Xie, Q. Ai, and Z. Yu, "Ultra-broadband selective absorber for near-perfect harvesting of solar energy," *J. Quantitative Spectrosc. Radiative Transfer*, vol. 266, 2021, Art. no. 107575, doi: 10.1016/j.jqsrt.2021.107575.

[19] S. Yue et al., "Ultra-broadband metamaterial absorber from ultraviolet to long-wave infrared based on CMOS-compatible materials," *Opt. Exp.*, vol. 28, pp. 31844–31861, 2020, doi: 10.1364/OE.403551.

[20] M. A. Naveed, R. M. H. Bilal, M. A. Baqir, M. M. Bashir, M. M. Ali, and A. A. Rahim, "Ultrawideband fractal metamaterial absorber made of nickel operating in the UV to IR spectrum," *Opt. Exp.*, vol. 29, pp. 42911–42923, 2021, doi: 10.1364/OE.446423.

[21] R. M. H. Bilal, M. A. Baqir, M. Hameed, S. A. Naqvi, and M. M. Ali, "Triangular metallic ring-shaped broadband polarization-insensitive and wide-angle metamaterial absorber for visible regime," *J. Opt. Soc. Amer. A*, vol. 39, pp. 136–142, 2022, doi: 10.1364/JOSAA.444523.

[22] H. Deng, L. Stan, D. A. Czaplewski, J. Gao, and X. Yang, "Broadband infrared absorbers with stacked double chromium ring resonators," *Opt. Exp.*, vol. 25, pp. 28295–28304, 2017, doi: 10.1364/OE.25.028295.

[23] F. Xu et al., "Broadband solar absorber based on square ring cross arrays of ZnS," *Micromachines*, vol. 12, 2021, Art. no. 909, doi: 10.3390/mi12080909.

[24] E. D. Palik, *Handbook of Optical Constants of Solids*. Cambridge, MA, USA: Academic Press.

[25] R. A. Shelby, D. R. Smith, and S. Schultz, "Experimental verification of a negative index of refraction," *Science*, vol. 292, pp. 77–79, 2001, doi: 10.1126/science.1058847.

[26] G. Fan et al., "Tailorable radio-frequency negative permittivity of titanium nitride sintered with different oxidation pretreatments," *Ceramics Int.*, vol. 43, no. 18, pp. 16980–16985, 2017, doi: 10.1016/j.ceramint.2017.09.105.

[27] E. D. Palik, *Handbook of Optical Constants of Solids II[M]*. Boston, MA, USA: Academic Press, 1991.

[28] H. Wang, V. P. Sivan, A. Mitchell, G. Rosengarten, P. Phelan, and L. Wang, "Highly efficient selective metamaterial absorber for high-temperature solar thermal energy harvesting," *Sol. Energy Mater. Sol. Cells*, vol. 137, pp. 235–242, 2015, doi: 10.1016/j.solmat.2015.02.019.

[29] M. Planck, "Über das gesetz der energieverteilung im normalspektrum," in *Von Kirchhoff Bis Planck*. Berlin, Germany: Springer, 1978, pp. 178–191.

[30] A. Yt, A. Xl, B. Ag, and Z. A. Yi, "Scalable-manufactured metal–insulator–metal based selective solar absorbers with excellent high-temperature insensitivity," *Appl. Energy*, vol. 281, 2021, Art. no. 116055, doi: 10.1016/j.apenergy.2020.116055.

[31] J. Kim, K. Han, and J. W. Hahn, "Selective dual-band metamaterial perfect absorber for infrared stealth technology," *Sci. Rep.*, vol. 7, no. 1, pp. 1–9, 2017, doi: 10.1038/s41598-017-06749-0.

[32] S. Cao, W. Yu, L. Zhang, C. Wang, X. Zhang, and Y. Fu, "Broadband efficient light absorbing in the visible regime by a metananoring array," *Annalen Der Physik*, vol. 526, pp. 112–117, 2014, doi: 10.1002/andp.201300198.

[33] U. Guler et al., "Local heating with lithographically fabricated plasmonic titanium nitride nanoparticles," *Nano Lett.*, vol. 13, pp. 6078–6083, 2013, doi: 10.1021/nl4033457.

[34] H. Zhang et al., "Metal-free plasmonic refractory core-shell nanowires for tunable all-dielectric broadband perfect absorbers," *Opt. Exp.*, vol. 28, no. 24, pp. 37049–37057, 2020, doi: 10.1364/OE.405625.

[35] G. Liu et al., "Near-unity, full-spectrum, nanoscale solar absorbers and near-perfect blackbody emitters," *Sol. Energy Mater. Sol. Cells*, vol. 190, pp. 20–29, 2019, doi: 10.1016/j.solmat.2018.10.011.

[36] R. M. H. Bilal, "Elliptical metallic rings-shaped fractal metamaterial absorber in the visible regime," *Sci. Rep.*, vol. 10, no. 1, pp. 1–12, 2020, doi: 10.1038/s41598-020-71032-8.

[37] N. T. Q. Hoa, P. H. Lam, P. D. Tung, T. S. Tuan, and H. Nguyen, "Numerical study of a wide-angle and polarization-insensitive ultrabroadband metamaterial absorber in visible and near-infrared region," *IEEE Photon. J.*, vol. 11, no. 1, Feb. 2019, Art. no. 4600208, doi: 10.1109/JPHOT.2018.2888971.

[38] P. T. Dang, J. Kim, T. K. Nguyen, K. Q. Le, and J.-H. Lee, "Ultra-broadband metamaterial absorber for high solar thermal energy conversion efficiency," *Physica B: Condens. Matter*, vol. 620, 2021, Art. no. 413261, doi: 10.1016/j.physb.2021.413261.

[39] Z. Zhou, Y. Chen, Y. Tian, J. Liang, and W. Yang, "Ultra-broadband metamaterial perfect solar absorber with polarization-independent and large incident angle-insensitive," *Opt. Laser Technol.*, vol. 156, 2022, Art. no. 108591, doi: 10.1016/j.optlastec.2022.108591.

[40] J. Liu, J. Chen, H. Liu, Y. Liu, and L. Zhu, "Numerical study of an ultra-broadband and polarization independence metamaterial cross-shaped fractal absorber," *Plasmonics*, vol. 15, pp. 1517–1524, 2020, doi: 10.1007/s11468-020-01156-0.

[41] H. Liu, M. Xie, Q. Ai, and Z. Yu, "Ultra-broadband selective absorber for near-perfect harvesting of solar energy," *J. Quantitative Spectrosc. Radiative Transfer*, vol. 266, 2021, Art. no. 107575, doi: 10.1016/j.jqsrt.2021.107575.